

Crystal-like thermal transport in amorphous carbon

Jaeyun Moon* and Zhiting Tian

Sibley School of Mechanical and Aerospace Engineering, Cornell University

(Dated: May 14, 2024)

Abstract

Thermal transport properties of amorphous carbon has attracted increasing attention due to its extreme thermal properties: It has been reported to have among the highest thermal conductivity for bulk amorphous solids up to $\sim 37 \text{ Wm}^{-1}\text{K}^{-1}$, comparable to crystalline sapphire ($\alpha\text{-Al}_2\text{O}_3$). Further, large density dependence in thermal conductivity demonstrates a potential for largely tunable thermal conductivity. However, mechanism behind the high thermal conductivity and its large density dependence remains elusive due to many variables at play. In this work, we perform large-scale ($\sim 10^5$ atoms) molecular dynamics simulations utilizing a machine learning potential based on neural networks. Through spectral decomposition of thermal conductivity which enables a quantum correction to classical heat capacity, we find that propagating vibrational excitations govern thermal transport in amorphous carbon ($\sim 100\%$ of thermal conductivity) in sharp contrast to the conventional wisdom that diffusive vibrational excitations dominate thermal transport in amorphous solids. Instead, this remarkable behavior resembles thermal transport in simple crystals. Moreover, our temperature dependent spectral diffusivity and velocity current correlation analyses reveal that the density dependent thermal conductivity originates from anharmonicity sensitive propagating excitations. Our work suggests a novel insight and design principle into developing mechanically hard, thermally conductive amorphous solids.

* To whom correspondence should be addressed; E-mail: jaeyun.moon@cornell.edu

I. INTRODUCTION

Vibrational properties of amorphous solids are of fundamental interest due to their anomalies compared to those of crystalline solids, including a Boson peak in the vibrational density of states [1, 2] and an excess heat capacity at cryogenic temperatures [3]. Combined with small average mean free paths on the order of interatomic distances [4], these anomalies suggest different characteristics of vibrational heat carriers from those of phonons in simple crystals. Prior seminal works have proposed to categorize these heat carriers in amorphous solids as propagating, diffusive, and localized vibrations depending on their transport mechanisms [5–7]. Propagating vibrational excitations are similar to phonons in that they have large mean free paths, thus transporting heat efficiently. Diffusive vibrations have ill-defined mean free paths below \sim interatomic distances and transport heat in a random walk manner. Localized vibrations are spatially localized and are often considered to contribute negligibly to thermal transport. These categorizations have been used to understand various thermal properties in numerous amorphous solids microscopically [8–15]. Consensus is that diffusive vibrations govern thermal transport in most amorphous solids due to large degrees of disorder hindering propagation of vibrations, leading to low thermal conductivity in dielectric amorphous solids ($\lesssim 1 \text{ Wm}^{-1}\text{K}^{-1}$).

Recently, amorphous carbon has drawn immense attention due to its remarkable mechanical and thermal properties [16–21]: Amorphous carbon with similar density to crystalline diamond (3.5 g cm^{-3} at 300 K) can achieve larger Young's modulus and hardness than those of crystalline diamond [21] and it has among the highest thermal conductivity reported for pure bulk amorphous solids up to $\sim 37 \text{ Wm}^{-1}\text{K}^{-1}$ at 300 K, comparable to that of many crystalline solids such as sapphire [18, 22]. Numerous experimental [18, 23–25] and computational works [26–29] have been conducted to elucidate the nature of atomic vibrations in amorphous carbon and to explore extreme thermal properties achievable in amorphous solids.

Prior measurements have shown that thermal conductivity has a strong positive correlation with mass density and sp^3 content, demonstrating that local atomic environment could be an important factor in thermal transport in amorphous carbon [18, 23–25]. However, thermal conductivity measurements of amorphous carbon vary significantly in literature (from ~ 1 to $\sim 37 \text{ Wm}^{-1}\text{K}^{-1}$) depending on many variables such as synthesis techniques and condi-

tions that lead to different densities, sample qualities, and possible crystallinities. Accurate and systematic atomic simulation studies are, thus, necessary to microscopically understand the thermal transport mechanisms in amorphous carbon and these will, in larger effect, play an essential role in understanding extreme thermal properties of amorphous solids.

Recent molecular dynamics simulations on amorphous carbon support the local structure (density and sp^3 content)-property (thermal conductivity) relationship [26–29]. By categorizing vibrations into propagating and diffusive modes, these simulation works have further reported that diffusive vibrations play a substantial role in thermal conduction in amorphous carbon (up to 70 % of thermal conductivity) at 300 K, a similar behavior observed in most other amorphous solids [13, 30, 31]. However, these simulations report: 1. unphysically large vibrational density of states at high frequencies above ~ 70 THz similar to hydrogen vibrational frequencies using simple empirical potentials [26], 2. small simulations cells, comprised of hundreds to thousands of atoms, not able to adequately include low frequency vibrations [26, 27, 29] 3. classical thermal conductivity values at room temperatures where phonon occupation is inaccurately described below Debye temperatures (~ 2300 K for amorphous carbon) [27, 28]. Despite these experimental and computational efforts, accurate understanding of thermal transport in amorphous carbon is still missing.

In this work, we perform molecular dynamics simulations of amorphous carbon using a machine learning potential based on neural networks. Large structures made of 110,592 atoms with varying densities from 3.0 to 3.8 g cm⁻³ are considered. With homogeneous non-equilibrium molecular dynamics descriptions of thermal conductivity based on a linear response theory, we decompose thermal conductivity into spectral contributions, enabling a quantum correction to the phonon occupation and heat capacity. The combination of machine learning potential with first principles accuracies, large structures, and quantum correction to heat capacity mitigates prior limitations mentioned before. By comparing with three widely used physical models and directly analyzing dispersions, we show that remarkably, propagating excitations govern thermal transport in amorphous carbon at room temperature (~ 100 % of thermal conductivity) similar to simple crystals but unlike most amorphous solids. This efficient mode of transport may explain the high thermal conductivity values observed in amorphous carbon. Further, through temperature dependent analysis, we find that large changes in density dependent thermal conductivity observed in amorphous carbon are due to anharmonicity sensitive propagating vibrational excitations

at low frequencies below ~ 10 THz. Our results provide novel insights and design principles into a possible mechanism behind achieving high thermal conductivity in amorphous solids.

II. RESULTS AND DISCUSSION

A. Amorphous carbon structures

Representative amorphous solid structures at 3.0, 3.3, and 3.5 g cm⁻³ are shown in Fig. 1A. Molecular dynamics simulation details are discussed in Methods. Number of atoms having four nearest neighbors (sp^3 -bonded) increase with density. A negligible number of atoms had two or five neighbors. Cutoff distance of 1.85 Å was used to determine atomic coordination numbers [32, 33]. A large, spatially homogenous increase in the number of sp^3 -bonded atoms with increase in density is clearly visible. All sp^3 -bonded atoms were subsequently identified for all structures and their density dependent population is plotted against prior experimental [25, 34–36] and computational works [32, 37] in Fig. 1B. While all data depict monotonic increase in sp^3 population with density, some empirical potentials such as Tersoff [32] and Brenner [37] underpredict the sp^3 population by more than a half compared to experimental values. Structures based on machine-learning potentials such as Gaussian approximation potential (GAP) [32] and NEP used here appear to have more consistent sp^3 population predictions against experiments and density functional theory (DFT) calculations. Resulting pair distribution function, $g(r) = \frac{1}{4\pi N n r^2} \sum_{i,j} \langle \delta(r - |\mathbf{r}_i - \mathbf{r}_j|) \rangle$, is demonstrated for our 3.5 g cm⁻³ structure along with a prior DFT structure [32] at the same density in Fig. 1C. Here, N is the number of atoms, n is the number density, \mathbf{r}_i is the atomic position of the i th atom, and the angled brackets denotes an ensemble average. As expected for an amorphous solid, broad peaks and valleys are observed. Consistent pair distribution functions are demonstrated between the two curves.

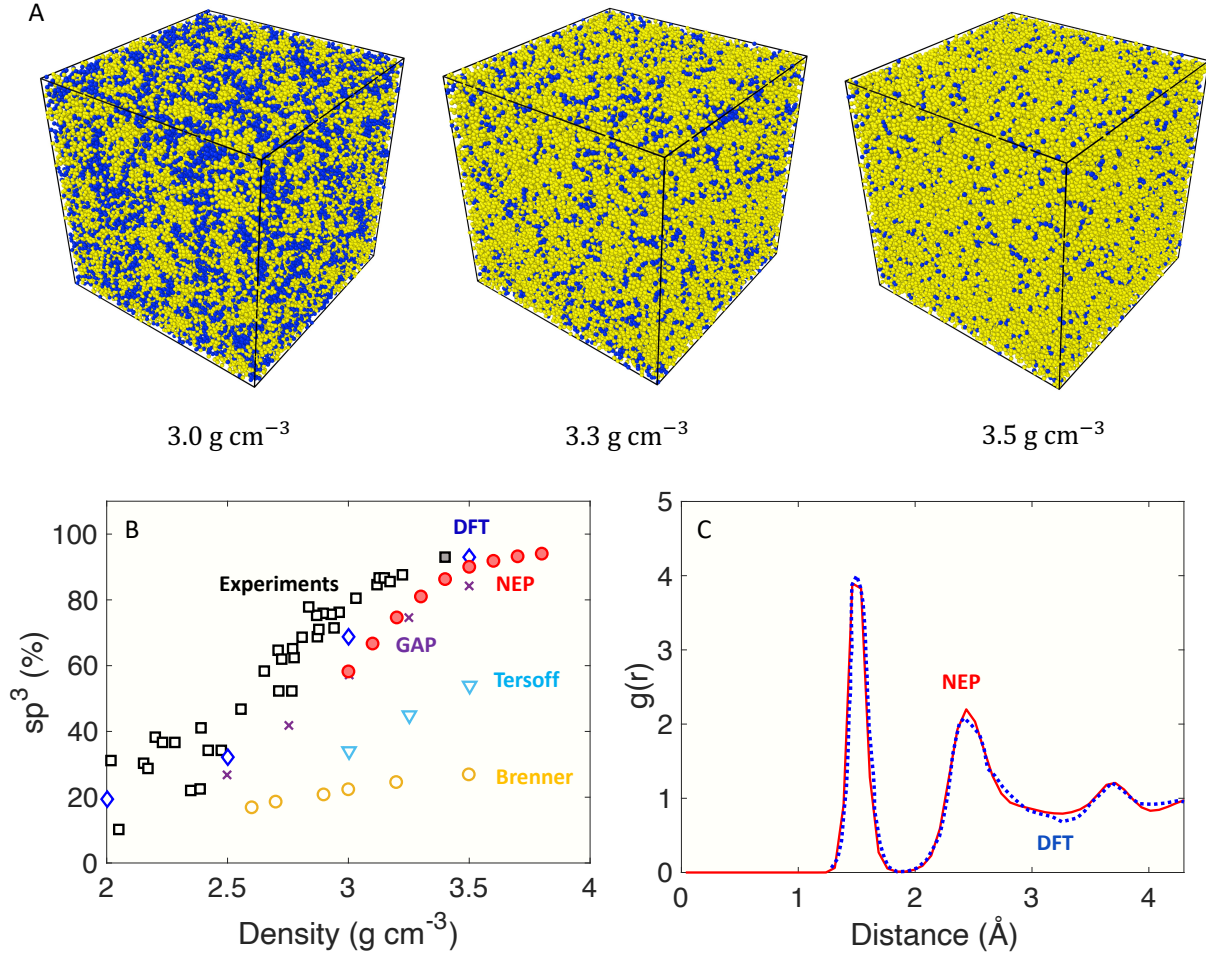


Figure 1. (A) Local atomic environment of tetrahedral amorphous carbon at different mass densities. Yellow and blue atoms denote atoms with sp^3 and sp^2 hybridizations, respectively. At 3.0, 3.3, and 3.5 $g\text{ cm}^{-3}$, 58.3, 81.0, and 90.1 % of atoms are sp^3 -bonded, respectively. (B) Density dependent sp^3 distributions of our NEP systems compared against previously reported values for various amorphous carbon systems from atomic simulations [32, 37] and experiments [21, 34–36]. (C) Pair distribution function of our system with 3.5 g cm^{-3} using the NEP potential (red curve) vs. prior literature using DFT [32] (blue curve).

B. Vibrations in amorphous carbon

Using these structures, we next examine their vibrational densities of states (DOS) using spectral velocity autocorrelations (see Fig. 2) [38–40]. Due to a large sample quantity typically required for density of states measurements, experimental measurement comparison is absent here. With increase in density, we observe a flatter DOS at low frequencies below 10 THz, which signifies higher Debye sound velocities (v_D) as DOS scales as v_D^{-3} . By fitting the Debye model of vibrational density of states below 5 THz, we obtain 12.97, 14.60, and 15.21 km s⁻¹ for the 3.0, 3.3, and 3.5 g cm⁻³ structures, respectively. Vibrational densities of states using the NEP potential appear to be more consistent with prior DFT calculations [33] while the DOS using a Tersoff potential [26] predicts a significant number of vibrations with frequencies higher than 50 THz. With the NEP potential, we then have structural and vibrational properties with first-principles accuracies for our large amorphous carbon structures.

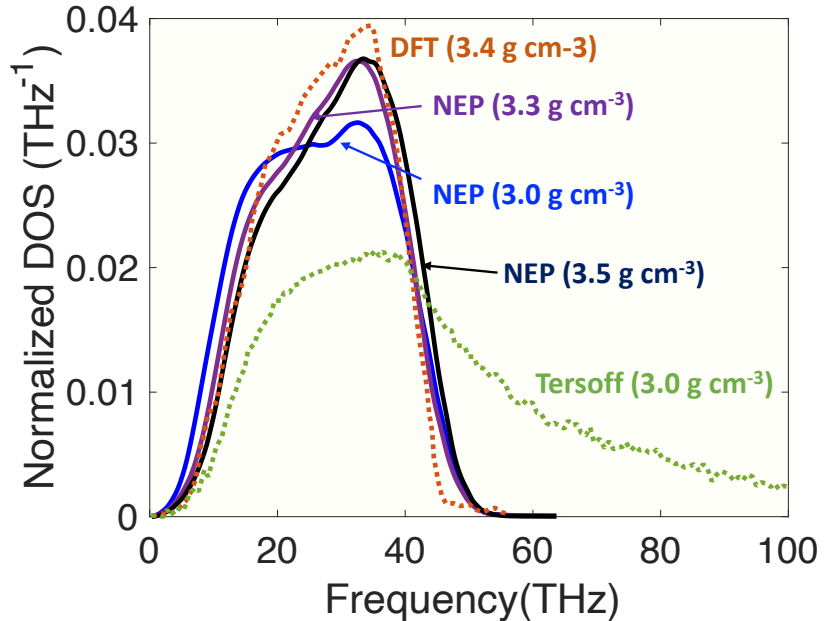


Figure 2. Vibrational densities of states (DOS) of various amorphous carbon systems. DOS for the 3.0, 3.3, and 3.5 g cm⁻³ structures studied here are shown as solid blue, purple, and black curves, respectively. DFT calculations (3.4 g cm⁻³) are shown as a brown dotted curve and DOS using Tersoff potential (3.0 g cm⁻³) is depicted as a green dotted curve.

C. Thermal conductivity and transport mechanisms

Thermal conductivity values for all the structures were then determined by homogeneous non-equilibrium molecular dynamics (HNEMD) [41, 42] (See Methods). Similar to the Green-Kubo (GK) formalism [43] in equilibrium molecular dynamics (EMD), the HNEMD method is based on a linear response theory. In HNEMD, independent phonon calculations are not required to obtain spectral thermal conductivity unlike other molecular dynamics based methodologies such as Green-Kubo modal analysis (GKMA) [8] and normal mode decomposition (NMD) [44] which limit the number of atoms due to large computational costs of constructing and diagonalizing dynamical matrices.

Classical and quantum corrected thermal conductivity of all systems studied here were plotted against experimental measurements and Green-Kubo thermal conductivity independently calculated here as shown in Fig. 3. Green-Kubo thermal conductivities were obtained by $k = \frac{V}{3k_B T} \int_0^\infty dt \langle \mathbf{J}(t) \cdot \mathbf{J}(0) \rangle$ where $\mathbf{J}(t)$ is the heat current. Classical thermal conductivity from HNEMD and GK thermal conductivity are within the errorbars of each other. There have been a lot of variations in the measured thermal conductivities for amorphous carbon depending on the synthesis techniques, thickness, and sample quality. Nonetheless, we observe that quantum corrected thermal conductivity for the amorphous carbon structures discussed here is on the same order of magnitude as measurements at 300 K [23, 24, 45].

To see the effect of the quantum correction to the heat capacity on the total thermal conductivity in amorphous carbon, spectral thermal conductivity and thermal conductivity accumulation functions of 3.0, 3.3, and 3.5 g cm⁻³ structures at 300 K are shown in Fig. 3B and 3C, respectively. It appears that the effect of quantum correction to the specific heat on thermal conductivity becomes prominent above ~ 7 THz. This is expected as $k_B T \sim 25$ meV or 6 THz at room temperature. At 300 K, the quantum correction to the heat capacity reduces the classical thermal conductivities by as much as 30 to 40 %, demonstrating the importance of considering quantum effects in these materials. Further, it is interesting to note that density affects spectral thermal conductivity of amorphous carbon drastically below ~ 10 THz while there is little to no effect above 10 THz. Therefore, our work reveals that density dependent thermal conductivity in amorphous carbon widely observed in literature at room temperature is likely due to changes in transport properties of these low frequency vibrations.

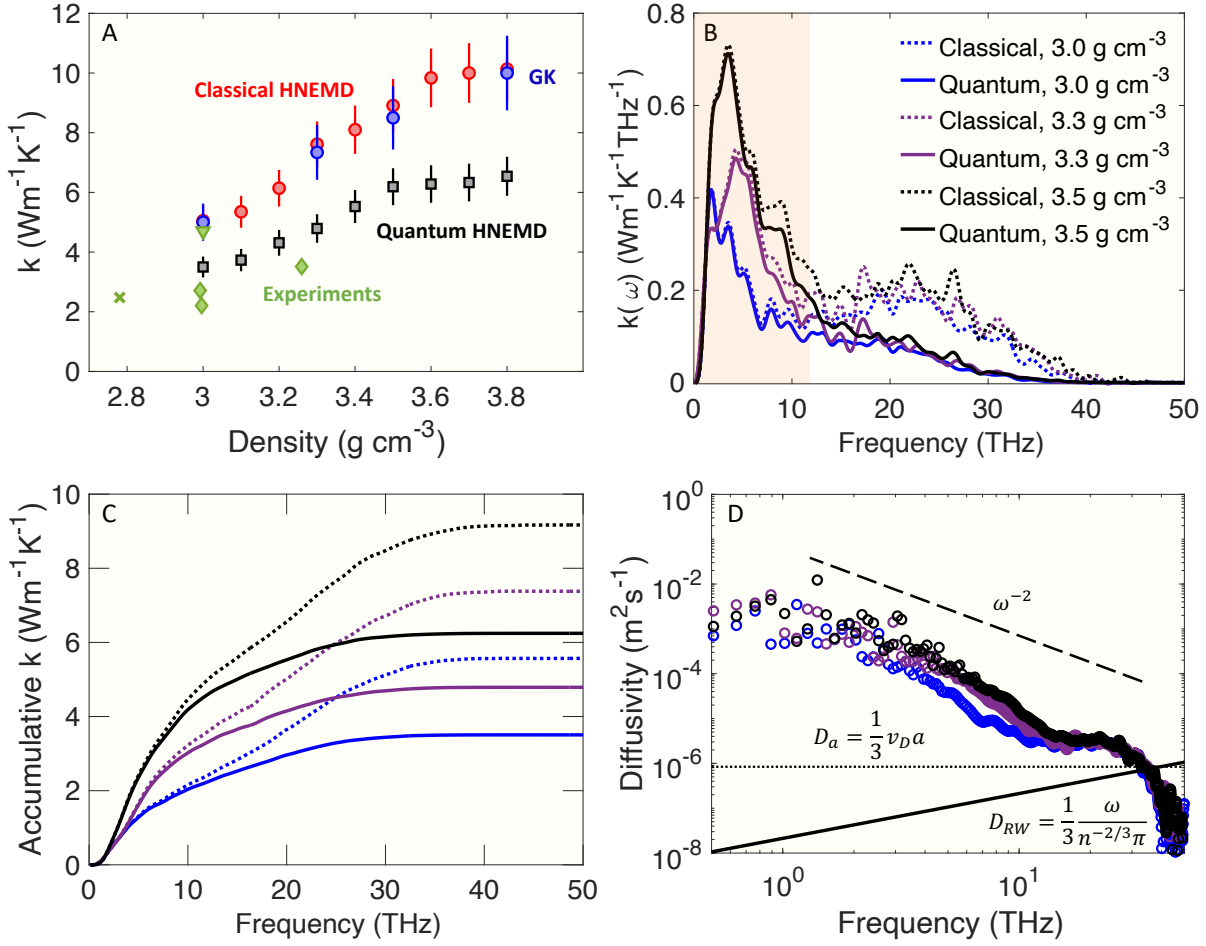


Figure 3. (A) Density dependent classical (red solid circles) and quantum mechanical (black solid squares) thermal conductivity at 300 K compared against thermal conductivity values using Green-Kubo formalism (blue solid circles) and available measurements (green symbols). Sample synthesis technique and thickness are: cross (filtered arc, 47 nm) [24], diamond (filtered cathodic vacuum arc, 18.5 to 100 nm) [23], and inverse triangle (filtered cathodic vacuum arc, 20 to 100 nm) [45] (B) Classical (solid curves) and quantum mechanical (dotted curves) spectral thermal conductivity. Shaded orange region highlights large density dependence in spectral thermal conductivity. (C) Thermal conductivity accumulation function of 3.0, 3.3, and 3.5 g cm^{-3} structures at 300 K. (D) Spectral diffusivity of 3.0, 3.3, and 3.5 g cm^{-3} structures at 300 K. Color schemes in (C) and (D) are the same as (B). Dashed line representing inverse quadratic power law is a guide to the eye. Dotted line represents diffusivity D_a when the mean free path is interatomic distance. Solid black line depicts a diffusivity based on a random-walk theory D_{RW} .

1. Characterization of propagating and diffusive vibrations

We next examine spectral thermal diffusivity values for the 3.0, 3.3, and 3.5 g cm⁻³ structures at 300 K obtained by $D(\omega) = \frac{k(\omega)}{C(\omega)DOS(\omega)}$ as plotted in Fig. 3D along with some widely used diffusivity models for amorphous materials. There currently exist a few different methods to distinguish propagating vibrations and diffusive vibrations: some methods require solving the dynamical matrices and subsequently examine normal mode shapes or properties (e.g. eigenvector periodicity [46]) and the other methods rely on physical models that describe propagating and diffusive vibrations. The first route is not computationally feasible here. Our systems ($\sim 10^5$ atoms) are more than an order of magnitude larger than typical numbers of atoms used for dynamical matrix calculations using simple empirical potentials in literature (10^3 to 10^4 atoms) [11, 12, 27]. Therefore, we resort to physical models describing propagating and diffusive vibrations.

The first model relies on how propagating wave lifetimes depend on frequency. At THz frequencies, lifetimes of propagating vibrations typically follow ω^{-2} . Prior works determined the frequency at which ω^{-2} dependence in lifetimes and diffusivity disappears as the transition frequency from propagating to diffusive vibrations in amorphous solids including amorphous carbon [11, 26, 31]. Using this criterion, we find that the transition frequency can be approximated to be around ~ 32 THz for these amorphous carbon structures (See Fig. S1 for more details in Supplementary Information).

The second physical model considers the lowest diffusivity (D_a) possible by a propagating wave where group velocity is sound velocity (here, we use the Debye velocity of ~ 14 km s⁻¹ as an average value) and mean free path is the interatomic distance, a [4]. The third model considered here considers maximum diffusivity for diffusive vibrations and is derived from a random walk theory [47] that has a linear dependence on frequency as $D_{RW} = \frac{1}{3} \frac{\omega}{\pi n^{2/3}}$ where n is the number density. If physically realistic, these two independent models should ideally merge at a certain frequency for amorphous carbon. These two criteria have been previously used in amorphous solids but also in complex crystals to determine propagating vs. diffusive normal modes that resulted in consistent thermal conductivity with experiments [12, 48–50]. Applying these two physical models lead to nearly identical crossover frequencies at remarkably high ~ 35 THz in amorphous carbon as shown in Fig. 3D.

Three physical models considered here consistently lead to remarkably high crossover

frequencies of \sim 30 to 35 THz. For these propagating vibrational excitations then, crisp dispersions with well-defined frequencies, group velocities, and mean free paths should be observed [1, 51–54]. Representative longitudinal and transverse dispersions for the 3.5 g cm⁻³ amorphous carbon structure are shown in Fig. 4A and B (see Methods for calculation details). At first glance, clear dispersions are demonstrated up to \sim 30 THz and \sim 20 THz for longitudinal and transverse excitations, respectively. By carefully fitting the single damped harmonic oscillator model at each wavevector shown in Fig. S2 in the Supplementary Information, we report mean free paths of longitudinal and transverse excitations in Fig. 4C. We find that propagating to diffusive crossover frequencies for longitudinal and transverse excitations are in a similar range as the other physical models at \sim 30 and 35 THz, respectively. Further, the mean free paths vary by nearly four orders of magnitude from \sim 1 THz to the crossover frequencies, similar to spectral thermal diffusivity calculated by HNEMD as shown in Fig. 3D.

All evidences based on the three physical models and dispersion analysis are pointing to the consequence that despite having intrinsically disordered structures, propagating vibrations that exist below 30 to 35 THz are responsible for thermal transport (\sim 100 % of thermal conductivity) in amorphous carbon at 300 K as demonstraed in Fig. 3C unlike most amorphous solids reported in literature where diffusive vibrations dominate thermal conduction [13, 55]. This behavior is remarkably similar to thermal transport in simple dielectric crystals. Our finding is in contrast with prior molecular dynamics predictions of amorphous carbon where a substantial contribution from diffusive vibrations is reported (up to 70 % of thermal conductivity) [26, 27]. We attribute this difference to a combination of three possible factors: 1. Simple empirical potentials may lack accuracy in predicting vibrational properties [26–28], 2. Prior simulations typically comprise of hundreds or thousands of atoms, not being able to include vibrations with long wavelengths and small frequencies adequately [26, 27, 29], and 3. Due to the lack of spectral decomposition of thermal conductivity, a quantum correction to the heat capacity was not possible, leading to overpredictions of high frequency mode contributions [27].

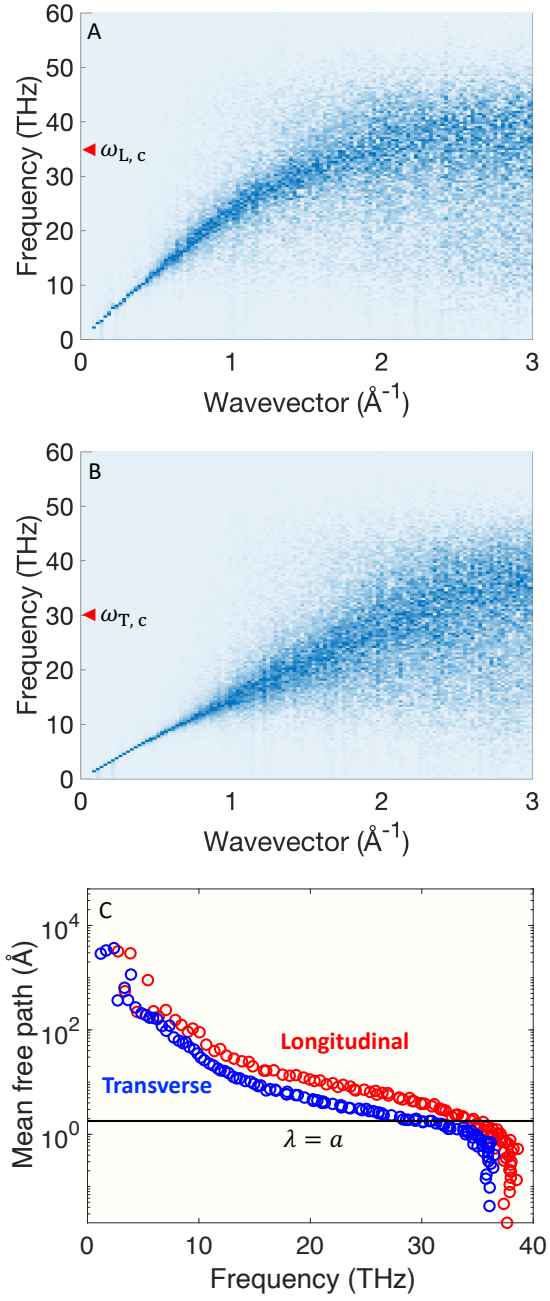


Figure 4. Wavevector and frequency resolved (A) longitudinal and (B) transverse velocity current correlations for the 3.5 g cm^{-3} structure. Estimated crossover frequencies from propagating to diffusive vibrations are noted as $\omega_{L,c}$ and $\omega_{T,c}$ for longitudinal and transverse directions, respectively. (C) Extracted mean free paths (λ) for both longitudinal (red circles) and transverse (blue circles) excitations. Horizontal black line is a guide to eye representing λ approaching interatomic distance (a) of amorphous carbon.

2. Temperature dependent thermal transport

So far, we have considered how thermal occupation affects thermal conductivity and the role of propagating vibrations in amorphous carbon at 300 K. We next explore the physical nature of scattering mechanisms of these propagating vibrations through examining temperature dependent thermal transport at 100, 300, and 500 K as shown in Fig. 5. Only the quantum corrected thermal conductivity values are plotted in Fig. 5A along with some prior measurements [23, 24]. Similar to density dependent thermal conductivity (see Fig. 3A), some differences between our predictions and measurements may arise from a variety of both experimental and computational origins including deposition techniques, sample thicknesses, and accuracy of the interatomic potential used here. A similar order of magnitude in thermal conductivity among the measurements and predictions is, nonetheless, shown. In all systems, a typical glass-like thermal conductivity temperature dependence is observed: thermal conductivity increases with increase in temperature.

Spectral diffusivity varies by ~ 6 orders of magnitude (see Fig. 3D). Therefore, diffusivity ratios for 100 K, 300 K, and 500 K are used as our metric of temperature effect for clear visualization. These ratios are representatively plotted for the 3.5 g cm^{-3} structure in Fig. 5B. Results for other amorphous carbon systems considered in this work are generally consistent with the 3.5 g cm^{-3} system and are not shown for redundancy. Above ~ 10 THz, both ratios fluctuate around unity, demonstrating that scattering mechanisms above ~ 10 THz are nearly temperature invariant and may originate from structural disorder in amorphous carbon. Below ~ 10 THz, we observe more significant temperature effects in the spectral diffusivity. Generally, D_{100K}/D_{500K} is greater than D_{100K}/D_{300K} in this frequency range, indicating that diffusivity monotonically decreases with increase in temperature. We attribute the temperature dependence of thermal diffusivity to anharmonic quasi-particle interactions in this frequency range. Similar trends are observed in independently calculated temperature dependent dispersion linewidths shown in Fig. S3. The trend that the ratios increase as frequency decreases is thought to originate from vibrations with larger periods (hence, larger wavelengths) becoming less sensitive to local disorders.

Our findings of the transition of scattering mechanisms from anharmonicity sensitive regime to disorder dominated regime are consistent with prior experimental works on various amorphous solids ranging from network systems [49, 56–59] to polymers [60, 61]: At low

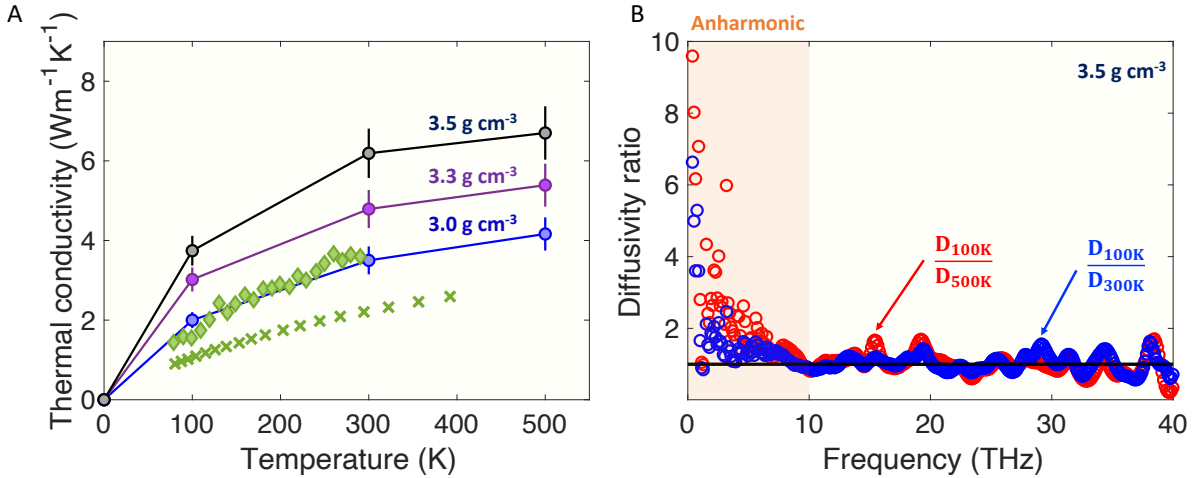


Figure 5. (A) Temperature dependent thermal conductivity for 3.0 (blue solid circles), 3.3 (purple solid circles), and 3.5 g cm^{-3} (black solid circles) structures compared against prior measurements (green solid diamond: filtered cathodic vacuum arc, 3.3 g cm^{-3} [23] and green cross: filtered arc, 2.8 g cm^{-3} [24]). These data and density dependent thermal conductivity data with the same symbols are from the same prior studies. (B) Spectral diffusivity ratios, D_{100K}/D_{500K} (red open circles) and D_{100K}/D_{300K} (blue open circles). Diffusivity ratio of unity is marked as black horizontal line as a guide to the eye.

frequencies below ~ 10 to 100 GHz, picosecond acoustics and Brillouin light scattering have shown strong temperature dependent mean free paths of acoustic excitations while negligible temperature dependence in the inelastic peak widths above peak frequency of 1 THz from inelastic X-ray and neutron scattering measurements have been reported. The high transition frequency of scattering mechanisms at ~ 10 THz observed here in amorphous carbon may be due to relatively high sound velocities [52] from strong C-C bonds. At a given wavevector, higher frequency acoustic waves are supported in amorphous carbon vs. those with low sound velocities.

Based on our density and temperature dependent vibrational and thermal characterizations, a novel insight into how density affects microscopic thermal transport in amorphous carbon emerges. It was observed in Fig. 2 that the enhancement in thermal conductivity with increase in density in amorphous carbon is mostly due to low frequency propagating vibrations below ~ 10 THz. From our temperature dependent diffusivity analysis, we further conclude that more specifically, anharmonicity sensitive propagating vibrations are respon-

sible for variations in thermal conductivity in amorphous carbon due to different densities studied here. We expect that our findings here can be extended to other amorphous solids, especially those with local tetrahedral orders including amorphous silicon, germanium, and silica. Direct verifications of our predictions may be possible through inelastic X-ray or neutron scattering measurements of vibrational density of states and dispersion of amorphous carbon.

III. CONCLUSIONS

Using a machine learning potential based on neural networks for large-scale amorphous carbon structures in molecular dynamics, we elucidate the microscopic mechanism behind high thermal conductivity values in amorphous carbon, among the highest in amorphous solids. Through spectral decomposition of thermal conductivity, quantum correction to the heat capacity, and dispersion analysis, we demonstrate that propagating vibrational excitations, present up to $30 \sim 35$ THz, dominate thermal transport in amorphous carbon at room temperature ($\sim 100\%$ of thermal conductivity). Further, temperature dependent analysis of thermal diffusivity and dispersion linewidths indicate that the origin of density dependent thermal conductivity is due to anharmonicity sensitive propagating vibrational excitations at low frequencies below ~ 10 THz, making connections between structure and property. Engineering anharmonicity sensitive vibrations could be key to achieving amorphous solids with high thermal conductivity. We have suggested an experimental approach based on inelastic scattering to test these predictions.

IV. METHODS

A. Molecular dynamics simulations

Crystal diamond of 110,592 atoms at various densities from 3.0 to 3.8 g cm $^{-3}$ were melted at 15,000 K for 30 ps, followed by quenching to an amorphous state at 1000 K at 100 K ps $^{-1}$ in NVT ensemble (constant number of atoms, volume, and temperature) using Graphics Processing Units Molecular Dynamics (GPUMD) [62]. Resulting structures were then annealed for 1 ns at 1000 K and were subsequently cooled to 300 K at 100 K ps $^{-1}$ in NVT. Using these seed structures, molecular dynamics outputs were recorded for 2 ns after initial

equilibration of 1 ns at desired temperatures (100, 300, and 500 K) under NVT. Our large structures result in more statistics of propagating vibrational excitations compared to prior molecular dynamics simulations with thousands of atoms [26, 27]. A timestep of 1 fs was used. Three runs with different initial velocities were carried out for better statistics for thermal and vibrational property calculations. Neuro-evolution potential (NEP), a neural network based machine-learning potential, was utilized to describe interatomic interactions with first-principles accuracies [62, 63].

B. Thermal conductivity calculations

In HNEMD, one applies an external driving force perturbation and examines the materials response (heat current) to it as

$$\mathbf{F}_i^{ext} = \mathbf{F}_e \cdot \mathbf{W}_i \quad (1)$$

where \mathbf{F}_e is the driving force parameter with the dimension of inverse length, $\mathbf{W}_i = \sum_{j \neq i} \frac{\partial U_j}{\partial \mathbf{r}_{ij}} \otimes \mathbf{r}_{ij}$ is the 3 by 3 virial tensor of an atom, \otimes represents a tensor product and U_j is the atomic potential energy. A small value of \mathbf{F}_e at $2 \times 10^{-4} \text{ \AA}^{-1}$ was used to ensure the system is in the linear response regime.

Instantaneous heat current is related to the virial tensor by

$$\mathbf{J}(t) = \sum_i \mathbf{W}_i \cdot \mathbf{v}_i. \quad (2)$$

Ensemble average of the heat current is then directly related to the driving force parameter and thermal conductivity by

$$\langle J^\alpha \rangle = TV \sum_\beta k^{\alpha\beta} F_e^\beta \quad (3)$$

where α and β represent Cartesian directions, T is temperature, and V is system volume. Thermal conductivity can therefore be determined from Eq. 1-3. For isotropic systems like amorphous carbon, isotropic thermal conductivity is expected. Therefore, we generally refer to thermal conductivity as k . We can further decompose thermal conductivity into spectral contributions through virial-velocity function $Q(t) = \sum_i \langle \mathbf{W}_i(0) \cdot \mathbf{v}_i(t) \rangle$ as

$$k(\omega) = \frac{2}{VTF_e} \int_{-\infty}^{\infty} Q(t) e^{i\omega t} dt. \quad (4)$$

Due to the classical nature of molecular dynamics simulations, atomic dynamics follows the Maxwell-Boltzmann distribution. With spectral thermal conductivity, one could, therefore,

apply a spectral ‘quantum correction’ to the occupation number and heat capacity such that

$$k_Q(\omega) = k(\omega) \frac{x^2 e^x}{(e^x - 1)^2}. \quad (5)$$

where $x = \frac{\hbar\omega}{k_B T}$, \hbar is the reduced Planck constant, and k_B is the Boltzmann constant [64]. HNEMD and spectral decompositions of thermal conductivity have been utilized in various materials including graphene [42] and amorphous silicon [64].

C. Dispersion analysis

Longitudinal and transverse dispersions from wavevector and frequency resolved velocity current correlations for amorphous carbon were obtained by [1, 12, 51, 52]

$$C_{L,T}(q, \omega) = \frac{q^2}{2\pi\omega^2 N} \int dt \langle \mathbf{j}_{L,T}(q, t) \cdot \mathbf{j}_{L,T}(-q, 0) \rangle e^{i\omega t} \quad (6)$$

where subscripts, L, T , refer to longitudinal or transverse branches, q is the wavevector, ω is the radial frequency, and $\mathbf{j}_{L,T}(q, t)$ is given by

$$\mathbf{j}_L(q, t) = \sum_i^N (\mathbf{v}_i(t) \cdot \hat{\mathbf{q}}) \hat{\mathbf{q}} e^{i\mathbf{q} \cdot \mathbf{r}_i(t)} \quad (7)$$

$$\mathbf{j}_T(q, t) = \sum_i^N (\mathbf{v}_i(t) - (\mathbf{v}_i(t) \cdot \hat{\mathbf{q}}) \hat{\mathbf{q}}) e^{i\mathbf{q} \cdot \mathbf{r}_i(t)} \quad (8)$$

with $\mathbf{v}_i(t)$, $\mathbf{r}_i(t)$, and $\hat{\mathbf{q}}$ representing atomic velocities, positions, and unit wavevector, respectively.

V. ACKNOWLEDGEMENT

Z.T. acknowledges the support of the Department of the Navy, Office of Naval Research under ONR award number N00014-22-1-2357. We are grateful for discussions with Dr. Lucas Lindsay. This work used the Extreme Science and Engineering Discovery Environment (XSEDE) Expanse under Allocation No. TG-MAT200012. This research used resources of the National Energy Research Scientific Computing Center (NERSC), a U.S. Department of Energy Office of Science User Facility located at Lawrence Berkeley National Laboratory, operated under Contract No. DE-AC02-05CH11231 using NERSC award BES-ERCAP0023621.

VI. AUTHOR CONTRIBUTIONS

J.M. conceived the research. J.M. performed simulations and data analysis. J.M. and Z.T. interpreted the results. J.M. wrote the paper with contributions from Z.T.

VII. COMPETING INTERESTS

The authors declare no competing interests.

**Supplementary Information for
Crystal-like thermal transport in amorphous carbon**

Jaeyun Moon* and Zhiting Tian

Sibley School of Mechanical and Aerospace Engineering, Cornell University

(Dated: May 14, 2024)

* To whom correspondence should be addressed; E-mail: jaeyun.moon@cornell.edu

I. DETERMINATION OF TRANSITION FREQUENCY FROM PROPAGATING TO DIFFUSING VIBRATIONS USING THE FREQUENCY POWER LAW

As discussed by prior works, determining the transition frequency through $D \sim \omega^{-2}$ is not exact and can only give us a ball park estimation. Some fluctuations in the diffusivities are demonstrated in our systems but it is clear that above ~ 32 THz, diffusivity no longer follows the power law and diverges as shown in Fig. S1.

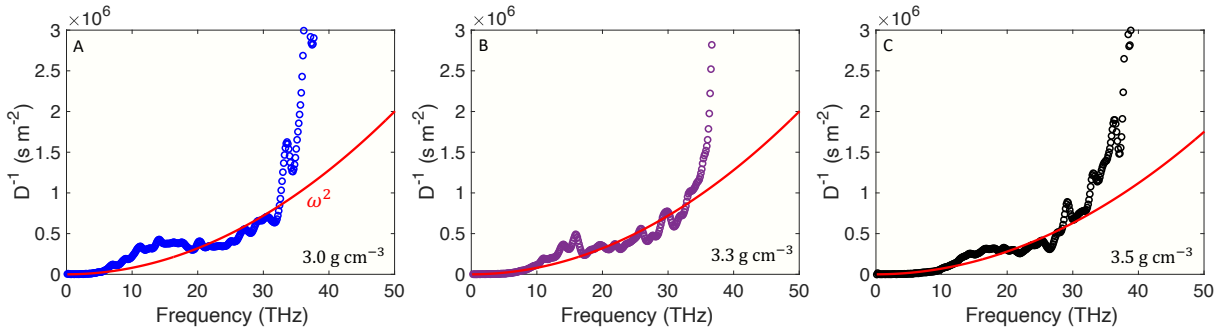


Fig. S1. Inverse of spectral diffusivity with frequency for the 3.0, 3.3, and 3.5 g cm^{-3} amorphous carbon structures studied.

II. COMMENT ON REF. [23] AND [26]

Temperature dependent thermal conductivity measurements from Ref. [23] shown as green solid diamond symbols in Fig. 4 of the main text have been cited to have the mass density of 3.0 g cm^{-3} in Ref. [26]. With this density, our thermal conductivity predictions at 3.0 g cm^{-3} (blue solid circles) in Fig. 4A are consistent with these measurements. However, it is our interpretation of the measurements from Ref. [23] that the reported mass density is $\sim 3.3 \text{ g cm}^{-3}$.

III. VELOCITY CURRENT CORRELATIONS ANALYSIS

Time Fourier transforms ($C_L(q, t)$ and $C_T(q, t)$) of the wavevector and frequency resolved velocity current correlation functions were fit by a single damped harmonic oscillator model, $C_{L,T}(q, t) = C_{L,T}(q, 0)e^{-\Gamma t/2} \cos \omega t$. Well-defined frequencies and relaxation times are demonstrated up to very high frequencies of ~ 30 to 35 THz as shown in Fig. S2.

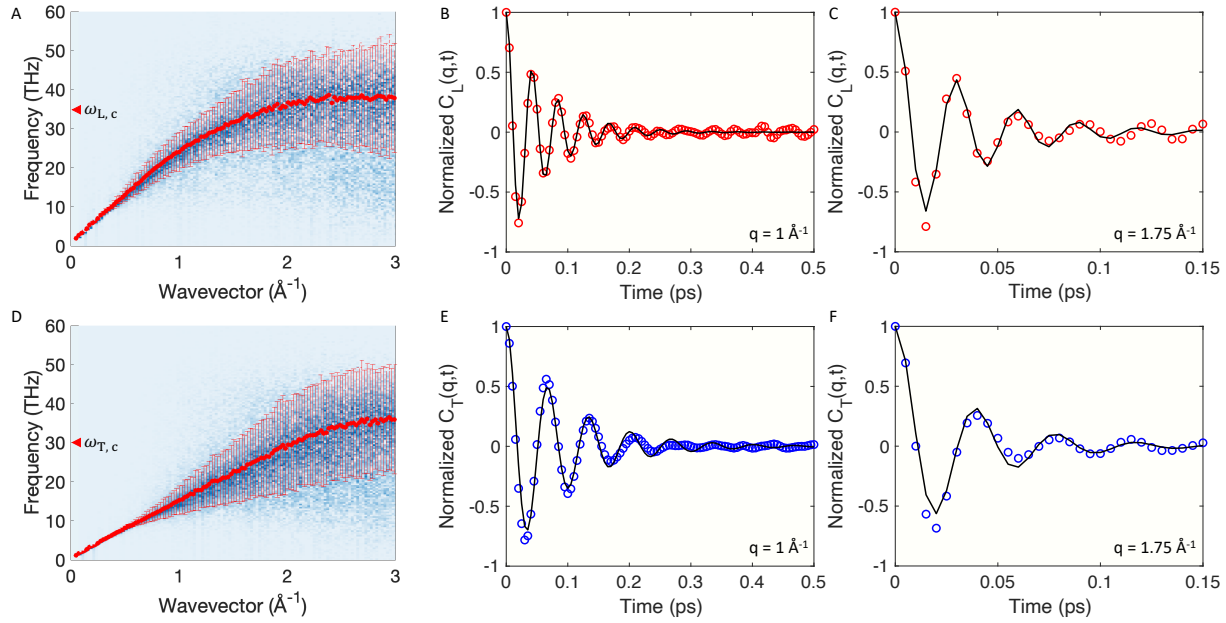


Fig. S2. Wavevector and frequency resolved (A) longitudinal and (D) transverse velocity current correlations for the 3.5 g cm^{-3} structure. Red solid circles with the errorbars represent peak frequencies and linewidths by fitting single damped harmonic oscillator. Clear dispersions are demonstrated up to $\sim 30 \text{ THz}$ in both longitudinal and transverse directions. Time resolved longitudinal velocity current correlations are shown at (B) 1 and (C) 1.75 nm^{-1} . Time resolved transverse velocity current correlations are shown at (E) 1 and (F) 1.75 nm^{-1} . Black curves are single damped harmonic oscillator model fits. Well-defined exponentially decaying oscillations are demonstrated at these wavevectors for both longitudinal and transverse directions.

Temperature dependent analysis of dispersion linewidths depict anharmonicity sensitive propagating excitations below $\sim 10 \text{ THz}$ as shown in Fig. S3, consistent with our thermal diffusivity analysis in the main text.

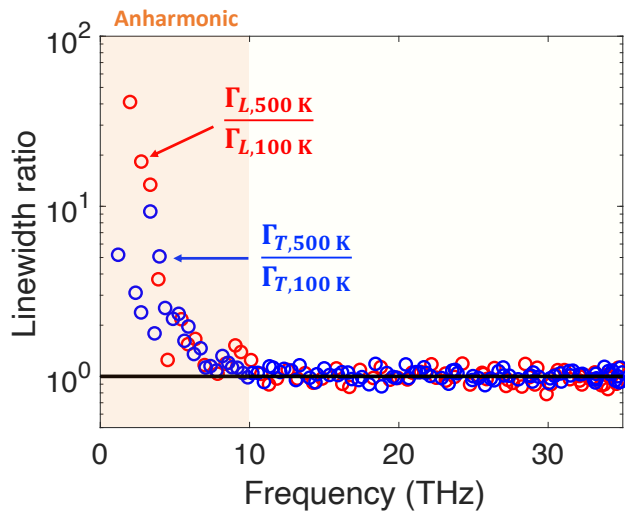


Fig. S3. Linewidth ratios for both longitudinal and transverse excitations demonstrate strong temperature dependence below ~ 10 THz for the 3.5 g cm^{-3} amorphous carbon structure.

-
- [1] H. Shintani and H. Tanaka, Universal link between the boson peak and transverse phonons in glass, *Nature Materials* **7**, 870 (2008).
 - [2] A. Chumakov, G. Monaco, A. Fontana, A. Bosak, R. Hermann, D. Bessas, B. Wehinger, W. Crichton, M. Krisch, R. Rüffer, G. Baldi, G. Carini Jr., G. Carini, G. D'Angelo, E. Gilioli, G. Tripodo, M. Zanatta, B. Winkler, V. Milman, K. Refson, M. Dove, N. Dubrovinskaia, L. Dubrovinsky, R. Keding, and Y. Yue, Role of Disorder in the Thermodynamics and Atomic Dynamics of Glasses, *Physical Review Letters* **112**, 10.1103/PhysRevLett.112.025502 (2014).
 - [3] R. C. Zeller and R. O. Pohl, Thermal conductivity and specific heat of noncrystalline solids, *Physical Review B* **4**, 2029 (1971).
 - [4] C. Kittel, Interpretation of the Thermal Conductivity of Glasses, *Physical Review* **75**, 972 (1949).
 - [5] P. B. Allen and J. L. Feldman, Thermal conductivity of glasses: Theory and application to amorphous Si, *Physical Review Letters* **62**, 645 (1989).
 - [6] P. B. Allen, J. L. Feldman, J. Fabian, and F. Wooten, Diffusons, locons and propagons: Character of atomic vibrations in amorphous Si, *Philosophical Magazine B* **79**, 1715 (1999).
 - [7] P. B. Allen, W. Garber, and L. Angelani, Character of Atomic Vibrations in a Lennard-Jones Glass (2003), arXiv:cond-mat/0307435.
 - [8] W. Lv and A. Henry, Direct calculation of modal contributions to thermal conductivity via Green-Kubo modal analysis, *New Journal of Physics* **18**, 013028 (2016).
 - [9] W. Lv and A. Henry, Examining the Validity of the Phonon Gas Model in Amorphous Materials, *Scientific Reports* **6**, 10.1038/srep37675 (2016).
 - [10] W. Lv and A. Henry, Non-negligible Contributions to Thermal Conductivity From Localized Modes in Amorphous Silicon Dioxide, *Scientific Reports* **6**, 35720 (2016).
 - [11] J. M. Larkin and A. J. H. McGaughey, Thermal conductivity accumulation in amorphous silica and amorphous silicon, *Physical Review B* **89**, 144303 (2014).
 - [12] J. Moon, B. Latour, and A. J. Minnich, Propagating elastic vibrations dominate thermal conduction in amorphous silicon, *Physical Review B* **97**, 10.1103/PhysRevB.97.024201 (2018).
 - [13] F. DeAngelis, M. G. Muraleedharan, J. Moon, H. R. Seyf, A. J. Minnich, A. J. H. McGaughey, and A. Henry, Thermal Transport in Disordered Materials, *Nanoscale and Microscale Ther-*

- mophysical Engineering (2018).
- [14] S. S. Sørensen, E. J. Pedersen, F. K. Paulsen, I. H. Adamsen, J. L. Laursen, S. Christensen, H. Johra, L. R. Jensen, and M. M. Smedskjaer, Heat conduction in oxide glasses: Balancing diffusons and propagons by network rigidity, *Applied Physics Letters* **117**, 031901 (2020).
 - [15] K. Aryana, D. A. Stewart, J. T. Gaskins, J. Nag, J. C. Read, D. H. Olson, M. K. Grobis, and P. E. Hopkins, Tuning network topology and vibrational mode localization to achieve ultralow thermal conductivity in amorphous chalcogenides, *Nature Communications* **12**, 2817 (2021), number: 1 Publisher: Nature Publishing Group.
 - [16] X. Zeng, R. Peng, Y. Yu, Z. Hu, Y. Wen, and L. Song, Pressure Effect on Elastic Constants and Related Properties of Ti₃Al Intermetallic Compound: A First-Principles Study, *Materials* **11**, 10.3390/ma11102015 (2018).
 - [17] Y. Lin, L. Zhang, H.-k. Mao, P. Chow, Y. Xiao, M. Baldini, J. Shu, and W. L. Mao, Amorphous Diamond: A High-Pressure Superhard Carbon Allotrope, *Physical Review Letters* **107**, 175504 (2011).
 - [18] Y. Shang, M. Yao, Z. Liu, R. Fu, L. Yan, L. Yang, Z. Zhang, J. Dong, C. Zhai, X. Hou, L. Fei, G. Zhang, J. Ji, J. Zhu, H. Lin, B. Sundqvist, and B. Liu, Enhancement of short/medium-range order and thermal conductivity in ultrahard sp³ amorphous carbon by C₇₀ precursor, *Nature Communications* **14**, 7860 (2023), number: 1 Publisher: Nature Publishing Group.
 - [19] S. Zhang, Z. Li, K. Luo, J. He, Y. Gao, A. V. Soldatov, V. Benavides, K. Shi, A. Nie, B. Zhang, W. Hu, M. Ma, Y. Liu, B. Wen, G. Gao, B. Liu, Y. Zhang, Y. Shu, D. Yu, X.-F. Zhou, Z. Zhao, B. Xu, L. Su, G. Yang, O. P. Chernogorova, and Y. Tian, Discovery of carbon-based strongest and hardest amorphous material, *National Science Review* **9**, nwab140 (2022).
 - [20] S. Zhang, Y. Wu, K. Luo, B. Liu, Y. Shu, Y. Zhang, L. Sun, Y. Gao, M. Ma, Z. Li, B. Li, P. Ying, Z. Zhao, W. Hu, V. Benavides, O. P. Chernogorova, A. V. Soldatov, J. He, D. Yu, B. Xu, and Y. Tian, Narrow-gap, semiconducting, superhard amorphous carbon with high toughness, derived from C₆₀ fullerene, *Cell Reports Physical Science* **2**, 100575 (2021).
 - [21] Y. Shang, Z. Liu, J. Dong, M. Yao, Z. Yang, Q. Li, C. Zhai, F. Shen, X. Hou, L. Wang, N. Zhang, W. Zhang, R. Fu, J. Ji, X. Zhang, H. Lin, Y. Fei, B. Sundqvist, W. Wang, and B. Liu, Ultrahard bulk amorphous carbon from collapsed fullerene, *Nature* **599**, 599 (2021), number: 7886 Publisher: Nature Publishing Group.
 - [22] D. G. Cahill, S.-M. Lee, and T. I. Selinder, Thermal conductivity of { χ }-Al₂O₃ and { α }-Al₂O₃

- wear-resistant coatings, *Journal of Applied Physics* **83**, 5783 (1998).
- [23] M. Shamsa, W. L. Liu, A. A. Balandin, C. Casiraghi, W. I. Milne, and A. C. Ferrari, Thermal conductivity of diamond-like carbon films, *Applied Physics Letters* **89**, 161921 (2006).
- [24] A. J. Bullen, K. E. O'Hara, D. G. Cahill, O. Monteiro, and A. von Keudell, Thermal conductivity of amorphous carbon thin films, *Journal of Applied Physics* **88**, 6317 (2000).
- [25] B. Shang, P. Guan, and J.-L. Barrat, Elastic avalanches reveal marginal behavior in amorphous solids, *Proceedings of the National Academy of Sciences* **117**, 86 (2020).
- [26] W. Lv and A. Henry, Phonon transport in amorphous carbon using Green – Kubo modal analysis, *Applied Physics Letters* **108**, 181905 (2016).
- [27] A. Giri, C. J. Dionne, and P. E. Hopkins, Atomic coordination dictates vibrational characteristics and thermal conductivity in amorphous carbon, *npj Computational Materials* **8**, 1 (2022), number: 1 Publisher: Nature Publishing Group.
- [28] I. Suarez-Martinez and N. A. Marks, Effect of microstructure on the thermal conductivity of disordered carbon, *Applied Physics Letters* **99**, 033101 (2011).
- [29] E. Minamitani, T. Shiga, M. Kashiwagi, and I. Obayashi, Relationship between local coordinates and thermal conductivity in amorphous carbon, *Journal of Vacuum Science & Technology A* **40**, 033408 (2022).
- [30] J. Moon and A. J. Minnich, Sub-amorphous thermal conductivity in amorphous heterogeneous nanocomposites, *RSC Advances* **6**, 105154 (2016).
- [31] Y. Zhou, A. Morshedifard, J. Lee, and M. J. Abdolhosseini Qomi, The contribution of propagons and diffusons in heat transport through calcium-silicate-hydrates, *Applied Physics Letters* **110**, 043104 (2017).
- [32] V. L. Deringer and G. Csányi, Machine learning based interatomic potential for amorphous carbon, *Physical Review B* **95**, 094203 (2017).
- [33] G. C. Sosso, V. L. Deringer, S. R. Elliott, and G. Csányi, Understanding the thermal properties of amorphous solids using machine-learning-based interatomic potentials, *Molecular Simulation* **44**, 866 (2018).
- [34] J. Schwan, S. Ulrich, H. Roth, H. Ehrhardt, S. R. P. Silva, J. Robertson, R. Samlenski, and R. Brenn, Tetrahedral amorphous carbon films prepared by magnetron sputtering and dc ion plating, *Journal of Applied Physics* **79**, 1416 (1996).
- [35] P. J. Fallon, V. S. Veerasamy, C. A. Davis, J. Robertson, G. A. J. Amaralunga, W. I. Milne,

- and J. Koskinen, Properties of filtered-ion-beam-deposited diamondlike carbon as a function of ion energy, *Physical Review B* **48**, 4777 (1993), publisher: American Physical Society.
- [36] A. C. Ferrari, A. Libassi, B. K. Tanner, V. Stolojan, J. Yuan, L. M. Brown, S. E. Rodil, B. Kleinsorge, and J. Robertson, Density, sp 3 fraction, and cross-sectional structure of amorphous carbon films determined by x-ray reflectivity and electron energy-loss spectroscopy, *Physical Review B* **62**, 11089 (2000).
- [37] L. Pastewka, P. Pou, R. Pérez, P. Gumbsch, and M. Moseler, Describing bond-breaking processes by reactive potentials: Importance of an environment-dependent interaction range, *Physical Review B* **78**, 161402 (2008), publisher: American Physical Society.
- [38] J. Moon, L. Lindsay, and T. Egami, Atomic dynamics in fluids: Normal mode analysis revisited, *Physical Review E* **108**, 014601 (2023), publisher: American Physical Society.
- [39] G. S. Grest, S. R. Nagel, and A. Rahman, Density of states and the velocity autocorrelation function derived from quench studies, *J. Chem. Phys.* **74**, 4 (1981).
- [40] J. Moon, *Heat Carriers in Liquids: An Introduction* (Springer, 2024).
- [41] Z. Fan, H. Dong, A. Harju, and T. Ala-Nissila, Homogeneous nonequilibrium molecular dynamics method for heat transport and spectral decomposition with many-body potentials, *Physical Review B* **99**, 064308 (2019).
- [42] A. J. Gabourie, Z. Fan, T. Ala-Nissila, and E. Pop, Spectral decomposition of thermal conductivity: Comparing velocity decomposition methods in homogeneous molecular dynamics simulations, *Physical Review B* **103**, 205421 (2021).
- [43] R. Kubo, The fluctuation-dissipation theorem, *Reports on Progress in Physics* **29**, 255 (1966).
- [44] A. J. McGaughey and J. M. Larkin, Predicting phonon properties from equilibrium molecular dynamics simulations, *Ann. Rev. Heat Transfer* **17**, 49 (2014).
- [45] G. Chen, P. Hui, and S. Xu, Thermal conduction in metalized tetrahedral amorphous carbon (ta-C) films on silicon, *Thin Solid Films* **366**, 95 (2000).
- [46] H. R. Seyf and A. Henry, A method for distinguishing between propagons, diffusions, and locons, *Journal of Applied Physics* **120**, 025101 (2016).
- [47] M. T. Agne, R. Hanus, and G. J. Snyder, Minimum thermal conductivity in the context of *diffuson* -mediated thermal transport, *Energy & Environmental Science* **11**, 609 (2018).
- [48] Y. Luo, X. Yang, T. Feng, J. Wang, and X. Ruan, Vibrational hierarchy leads to dual-phonon transport in low thermal conductivity crystals, *Nature Communications* **11**, 2554 (2020).

- [49] T. Kim, J. Moon, and A. J. Minnich, Origin of micrometer-scale propagation lengths of heat-carrying acoustic excitations in amorphous silicon, *Physical Review Materials* **5**, 065602 (2021), publisher: American Physical Society.
- [50] Z. Cai, S. Lin, M.-R. Ahmadian-Yazdi, and C. Zhao, Diffusion-Dominated and Ultra Defect-Tolerant Two-Channel Thermal Transport in Hybrid Halide Perovskites, *Advanced Functional Materials* , 2307648 (2023).
- [51] G. Monaco and S. Mossa, Anomalous properties of the acoustic excitations in glasses on the mesoscopic length scale, *Proceedings of the National Academy of Sciences* **106**, 16907 (2009).
- [52] J. Moon, R. P. Hermann, M. E. Manley, A. Alatas, A. H. Said, and A. J. Minnich, Thermal acoustic excitations with atomic-scale wavelengths in amorphous silicon, *Physical Review Materials* **3**, 065601 (2019).
- [53] F. Sette, M. H. Krisch, C. Masciovecchio, G. Ruocco, and G. Monaco, Dynamics of glasses and glass-forming liquids studied by inelastic X-ray scattering, *Science* **280**, 1550 (1998).
- [54] A. Fiorentino, P. Pegolo, and S. Baroni, Hydrodynamic finite-size scaling of the thermal conductivity in glasses, *npj Computational Materials* **9**, 1 (2023), publisher: Nature Publishing Group.
- [55] M. C. Wingert, J. Zheng, S. Kwon, and R. Chen, Thermal transport in amorphous materials: a review, *Semiconductor Science and Technology* **31**, 113003 (2016).
- [56] G. Baldi, V. Giordano, B. Ruta, R. Dal Maschio, A. Fontana, and G. Monaco, Anharmonic Damping of Terahertz Acoustic Waves in a Network Glass and Its Effect on the Density of Vibrational States, *Physical Review Letters* **112**, 10.1103/PhysRevLett.112.125502 (2014).
- [57] C. Masciovecchio, G. Baldi, S. Caponi, L. Comez, S. Di Fonzo, D. Fioretto, A. Fontana, A. Gessini, S. C. Santucci, F. Sette, G. Viliani, P. Vilmercati, and G. Ruocco, Evidence for a Crossover in the Frequency Dependence of the Acoustic Attenuation in Vitreous Silica, *Physical Review Letters* **97**, 10.1103/PhysRevLett.97.035501 (2006).
- [58] G. Ruocco and F. Sette, High-frequency vibrational dynamics in glasses, *Journal of Physics: Condensed Matter* **13**, 9141 (2001).
- [59] B. Rufflé, G. Guimbretière, E. Courtens, R. Vacher, and G. Monaco, Glass-Specific Behavior in the Damping of Acousticlike Vibrations, *Physical Review Letters* **96**, 10.1103/PhysRevLett.96.045502 (2006).
- [60] F. Sette, G. Ruocco, M. Krisch, U. Bergmann, C. Masciovecchio, V. Mazzacurati, G. Signorelli,

- and R. Verbeni, Collective Dynamics in Water by High Energy Resolution Inelastic X-Ray Scattering, *Physical Review Letters* **75**, 850 (1995).
- [61] C. Masciovecchio, A. Gessini, S. Di Fonzo, L. Comez, S. C. Santucci, and D. Fioretto, Inelastic Ultraviolet Scattering from High Frequency Acoustic Modes in Glasses, *Physical Review Letters* **92**, 247401 (2004).
- [62] Z. Fan, Y. Wang, P. Ying, K. Song, J. Wang, Y. Wang, Z. Zeng, K. Xu, E. Lindgren, J. M. Rahm, A. J. Gabourie, J. Liu, H. Dong, J. Wu, Y. Chen, Z. Zhong, J. Sun, P. Erhart, Y. Su, and T. Ala-Nissila, GPUMD: A package for constructing accurate machine-learned potentials and performing highly efficient atomistic simulations, *The Journal of Chemical Physics* **157**, 114801 (2022).
- [63] Z. Fan, Z. Zeng, C. Zhang, Y. Wang, K. Song, H. Dong, Y. Chen, and T. Ala-Nissila, Neuroevolution machine learning potentials: Combining high accuracy and low cost in atomistic simulations and application to heat transport, *Physical Review B* **104**, 104309 (2021), publisher: American Physical Society.
- [64] Y. Wang, Z. Fan, P. Qian, M. A. Caro, and T. Ala-Nissila, Quantum-corrected thickness-dependent thermal conductivity in amorphous silicon predicted by machine learning molecular dynamics simulations, *Physical Review B* **107**, 054303 (2023), publisher: American Physical Society.